ORIGINAL PAPER

Magnetic and Optical Properties of $CoFe_2O_4$ Nanoparticles Synthesized by Reverse Micelle Microemulsion Method

Paveena Laokul[1] · Sathakan Arthan[1] · Santi Maensiri[2] · Ekaphan Swatsitang[3,4]

Abstract $CoFe_2O_4$ nanoparticles were successfully synthesized by reverse micelle microemulsion method. The X-ray diffraction (XRD) results show that all samples have a spinel ferrite structure with calculated crystallite sizes in the range of 3.6–21.7 nm. Increasing calcination temperature from 650 to 900 °C can increase the crystallization of the powders. Transmission electron microscopy (TEM) images reveal the spherical shape of nanoparticles with serious agglomeration. Particle sizes of the samples calcined at 700, 800, and 900 °C estimated from TEM images are 9.7 ± 2.1, 10.6 ± 1.6, and 14.9 ± 0.4 nm, respectively. The UV–visible spectroscopy results show a decrease in the energy band gap (E_g) from 4.3 to 3.0 eV with increasing crystallite size. The room temperature magnetic properties of the calcined $CoFe_2O_4$ nanoparticles performed by vibrating sample magnetometry (VSM) indicate ferrimagnetic behavior in all samples. In addition, the specific magnetizations measured at the maximum field of ± 30 kOe (M_{max}) and coercivity (H_c) are increased with increasing calcination temperature. These characteristics of the prepared $CoFe_2O_4$ nanoparticles make them a promising magnetically separable photocatalyst for wastewater treatment.

Keywords Cobalt ferrite · Spinel structure · Nanoparticles · Magnetic properties · Optical properties

✉ Paveena Laokul
paveena@msu.ac.th; paveena.kku@gmail.com

1 Department of Physics, Faculty of Science Mahasarakham University, Kantharawichai Mahasarakham, 44150, Thailand

2 School of Physics, Institute of Science, Suranaree University of Technology, Nakhon Ratchasima, 30000, Thailand

3 Department of Physics, Faculty of Science Khon Kaen University, Khon Kaen, 40002, Thailand

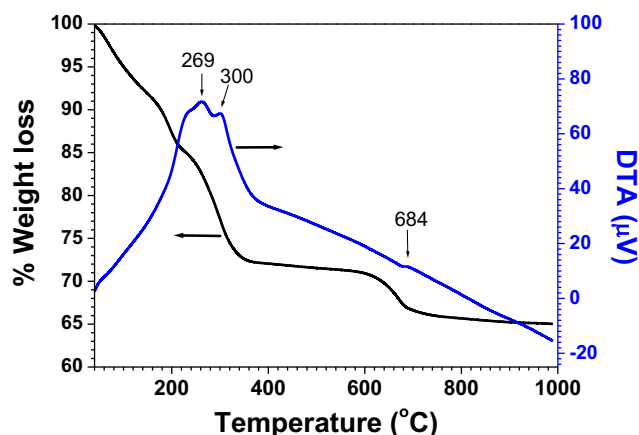4 Integrated Nanotechnology Research Center, Khon Kaen University, Khon Kaen, 40002, Thailand

1 Introduction

Spinel ferrites with the formula of MFe_2O_4, where M represents a divalent metal ion, have shown great potential for applications due to their unique optical, electrical, and magnetic properties. These materials are technologically important and have been used in many applications including magnetic recording media and magnetic fluids for the storage and/or retrieval of information, magnetic resonance imaging (MRI) enhancement, catalysis, magnetically guided drug delivery, sensors, pigments, etc. [1–3]. In the last decade, the use of ferrite nanoparticles as catalysts in organic transformations has attracted considerable interest [4]. In addition, ferrites are magnetic in nature, giving them added advantage of easy recovery after photocatalytic reaction [5–7]. Cubic structure $CoFe_2O_4$ has been widely studied due to its high electromagnetic performance, excellent chemical stability, mechanical hardness and high cubic magnetocrystalline anisotropy. As a result, $CoFe_2O_4$ is used in many fields of application such as audio/video tape, high-density digital recording disk, etc. [8]. Nevertheless, other properties such as optical properties, optoelectronics, photocatalytic activity, etc. of $CoFe_2O_4$ nanoparticles still need further study for functional applications. However, many potential applications of ferrites depend strongly on their particle size and morphology; it is then attractive to researchers with the attempt to develop a novel technique which can control particle size and morphology of

Fig. 1 TG-DTA curves of the $CoFe_2O_4$ precursor powder

ferrite particles. Nowadays, there are several techniques which can be used to prepare magnetic nanoparticles such as sol–gel, co-precipitation, hydrothermal, laser pyrolysis, and microemulsion methods [9–15]. Among these techniques, microemulsion is found to be an alternative one that relies on a stabilizing agent in order to prevent the aggregation of the resultant $CoFe_2O_4$ nanoparticles [16].

In this study, $CoFe_2O_4$ nanoparticles were synthesized by the microemulsion method [17]. The reagent and ionic surfactant used are cobalt(II) chloride hexahydrate, iron(III) chloride hexahydrate, and dioctyl sulfosuccinate sodium salt (AOT), respectively. Thermal behavior of the as-prepared powder was analyzed using thermogravimetric–differential thermal analysis (TG-DTA). The influence of calcination temperature on crystallinity, optical properties, and room temperature magnetic properties of the prepared $CoFe_2O_4$ nanoparticles was investigated using X-ray diffraction (XRD), UV–visible spectroscopy, and vibrating sample magnetometry (VSM), respectively. The particle size and microstructure of the calcined samples were further studied by transmission electron microscopy (TEM)
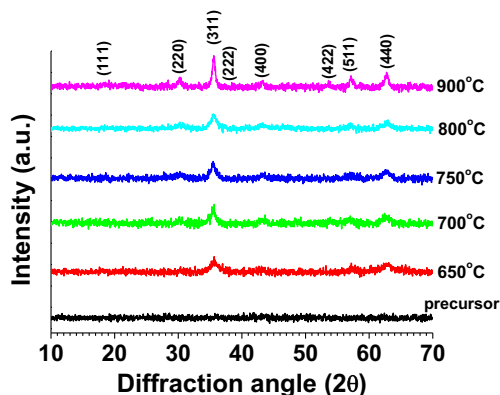

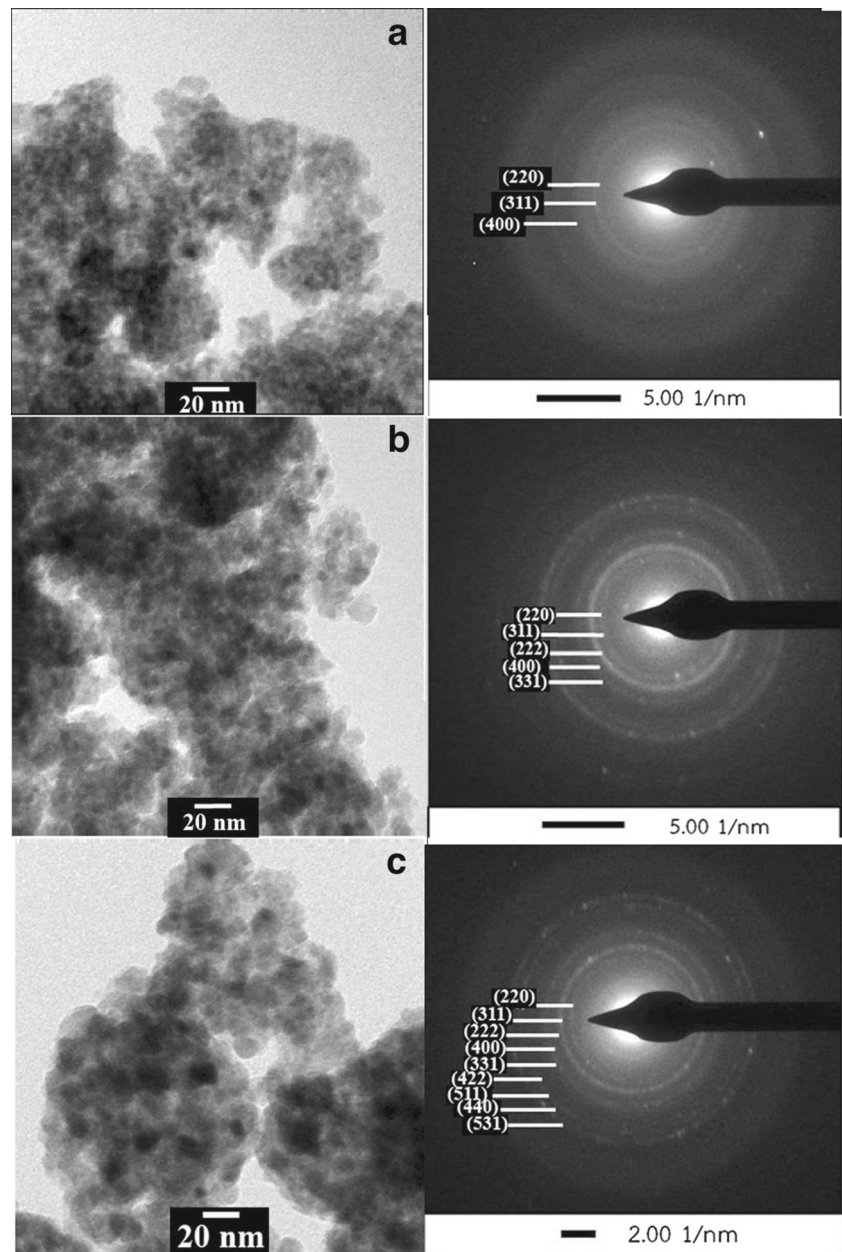**Fig. 2** XRD patterns of the $CoFe_2O_4$ precursor and nanoparticles calcined at different temperatures

2 Experimental

In this work, cobalt(II) chloride hexahydrate, $CoCl_2 \cdot 6H_2O$ (sigma–Aldrich), iron(III) chloride hexahydrate, $FeCl_3 \cdot 6H_2O$ (sigma–Aldrich), dioctyl sodium sulfosuccinate, $C_{20}H_{37}NaO_7S$ or AOT (sigma–Aldrich, 98 %), an oil phase as n-hexane (BDH Prolabo, HPLC grade 99 %), and precipitation agent as ammonium hydroxide (NH_4OH; Panreac, 30 %) were used to prepare $CoFe_2O_4$ powder. All of the reactants are of analytical grade. Two types of microemulsion systems, ME1 and ME2, were separately prepared. The first system, ME1, was prepared by mixing microemulsion solution (0.5 M AOT in n-hexane) into a proper amount of 10 % NH_4OH aqueous solution. In the second system, ME2, aqueous solution of $CoCl_2 \cdot 6H_2O$ and $FeCl_3 \cdot 6H_2O$, with a stoichiometric ratio (Co^{2+}:Fe^{3+}) of 1:2, was mixed with microemulsion solution to form a dispersed microemulsion aqueous phase. Appropriate amounts of ME1 and ME2 aqueous media were mixed together with continuous magnetic stirring at 40 °C for 2 h until a red-brown $CoFe_2O_4$ precursor layer was formed at the bottom. The $CoFe_2O_4$ precursor powder was separated by centrifugation at 13000 rpm for 15 min. The obtained product was subsequently washed with deionized water and methanol and was further dried at 70 °C in an oven for 48 h. It was then subjected to thermogravimetric–differential thermal analysis (Pyris Diamond TG-DTA, Perkin Elmer Instrument, USA) in the temperature range of 40–1000 °C in air using a heating rate of 10 °C/min to determine the temperature of possible decomposition and phase change. In order to obtain cubic structure $CoFe_2O_4$ nanoparticles, the as-prepared product was subjected to calcination at the temperatures of 650, 700, 750, 800, and 900 °C in air for 2 h. All calcined samples were characterized by X-ray diffraction (D2 Phaser, Bruker, Germany), transmission electron microscopy (Tecnai G29, FEI, USA), UV–visible spectroscopy (UV-1700, Shimadzu, Japan), and vibrating sample magnetometry (VSM, VersaLab, Quantum Design).

3 Results and Discussion

The results of TG-DTA measurement are shown in Fig. 1. From the TGA curve, the weight loss of the precursor powder with increasing temperature from 40 to 320 °C is associated with exothermic peaks of DTA at around 270 and 300 °C; then, it is slowly decreased in the temperature range of 320–680 °C and no further weight loss can be observed at the temperature above 680 °C. It is suggested that the exotherm below 300 °C is due to free adsorbed water and n-hexane [18]. In addition, the exothermic peak at about 680 °C may be attributed to the crystallization of an amorphous phase into the cubic phase of $CuFe_2O_4$.

Fig. 3 TEM micrographs and SAED patterns of CoFe$_2$O$_4$ nanoparticles calcined in air at **(a)** 700, **(b)** 800, and **(c)** 900 °C for 2 h

The technique of XRD was used to determine phase composition and microstructure of the CoFe$_2$O$_4$ precursor and the powders calcined at temperatures of 650, 700, 750, 800, and 900 °C. As shown in Fig. 2, the XRD patterns indicate that the as-prepared precursor powder is amorphous whereas the samples calcined at 650 °C and above are crystalline CoFe$_2$O$_4$ with the diffraction peaks of (111), (220), (311), (222), (400), (422), (511), and (440) planes corresponding to those reported in the standard data JCPDS no. 78-1970. The increase of XRD intensity indicates that higher calcination temperature can result in higher crystallinity that originates from the increment of crystalline volume ratio due to particle size enlargement of the

CoFe$_2$O$_4$ nuclei [19]. The average crystallite size (D) of the samples can be determined by Scherrer's equation [20], $D = 0.89\lambda/\beta\cos\theta$, where λ is the wavelength of X-ray radiation, θ is the diffraction angle, and β is the line broadening, after subtracting the instrumental line broadening, at half the maximum intensity (FWHM) of the most intense peak corresponding to the (311) plane. The average crystallite size of the calcined samples is summarized in Table 1. The results reveal that calcination temperature plays an important role in the formation of the spinel crystal structure and the controlling of the crystallite size [10]. From the table, crystallite size variation of the sample calcined in the temperature range of 650–900 °C is lower than those

Fig. 4 Room temperature absorbance spectra of CoFe$_2$O$_4$ nanoparticles calcined at **(a)** 700, **(b)** 750, **(c)** 800, and **(d)** 900 °C
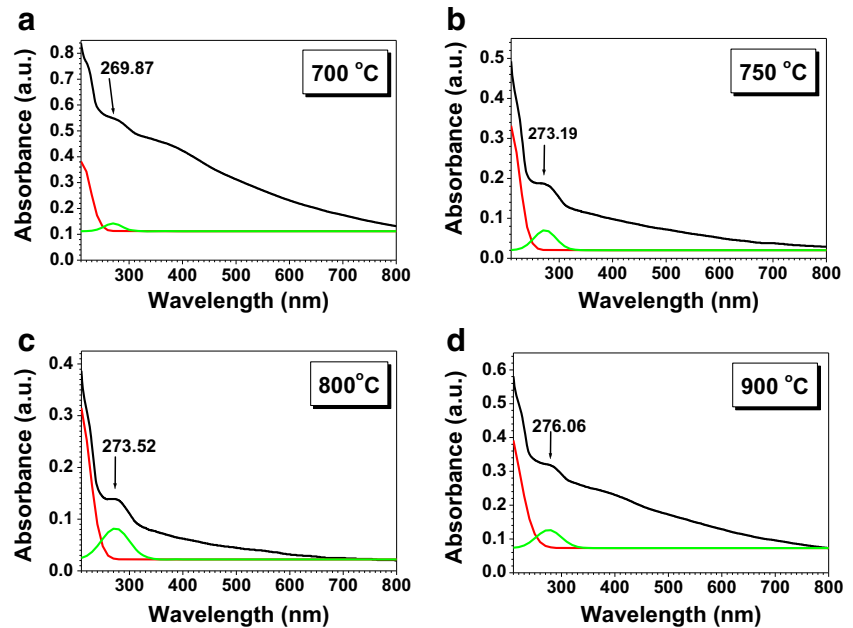
reported in literature, and it is possible due to the different synthesis method used for the preparation of CoFe$_2$O$_4$ nanoparticles.

TEM bright field images with corresponding selected area electron diffraction (SAED) patterns of CoFe$_2$O$_4$ nanoparticles calcined at 700, 800 and 900 °C are shown in Fig. 3. The bright field TEM images reveal that the synthesized CoFe$_2$O$_4$ nanoparticles are spherical in shape with serious agglomeration. The average particle sizes of the samples calcined at 700, 800 and 900 °C measured from

TEM micrographs are approximately 10, 11, and 15 nm, respectively. It is noted that the particle size of CoFe$_2$O$_4$ increases with increasing calcination temperature. The tendency of particle size variation is in good agreement with those evaluated by X-ray diffraction line broadening as shown in Table 1. Particle size enlargement at higher calcination temperature of CoFe$_2$O$_4$ and other ferrite systems is due to grain growth observed previously in other works [3, 21, 22]. The different values of particle size investigated by TEM and crystallite size evaluated by XRD techniques

Fig. 5 Plots of $(\alpha h\nu)^2$ as a function of photon energy ($h\nu$) of nanocrystalline CoFe$_2$O$_4$ samples calcined at **(a)** 700, **(b)** 750, **(c)** 800, and **(d)** 900 °C
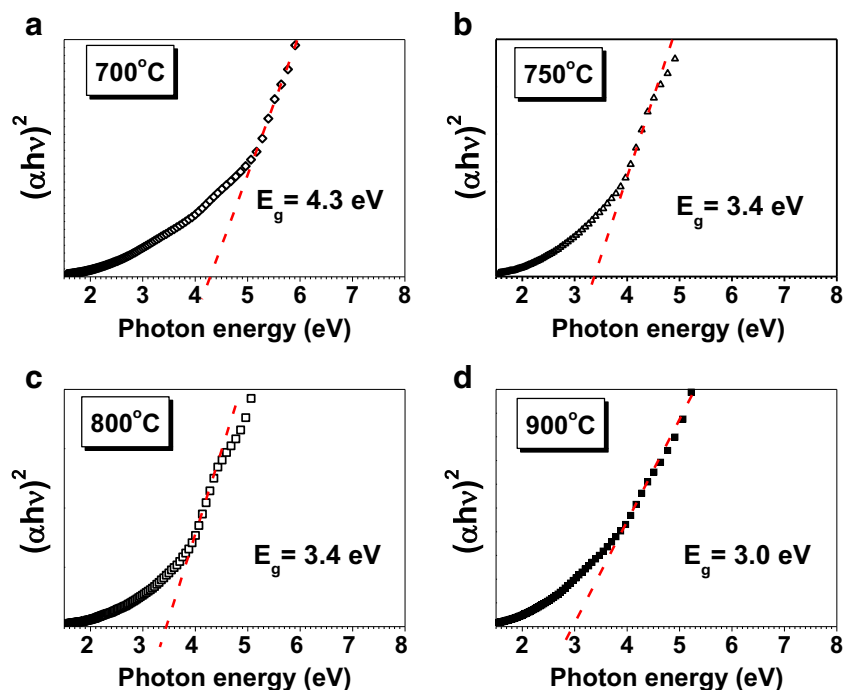
Table 1 Summary of crystallite size, particle size, direct band gap (E_g), specific magnetization at the maximum field (M_{max}), and coercivity (H_c) of nanocrystalline $CoFe_2O_4$ calcined at different temperatures

Calculation	Crystallite Size	Particle Size	E_g	Magnetization	Coercivity
Temperature (°C)	(nm)	(nm)	(eV)	(emu/g)	(Oe)
650	3.6	–	–	27.46	116.88
700	5.3	9.7 ± 2.1	4.3	31.99	142.86
750	6.9	–	3.4	38.25	181.82
800	9.2	10.6 ± 1.6	3.4	40.11	311.69
900	21.7	14.9 ± 0.4	3.0	57.40	1266.24

may be due to the agglomeration of ultrafine $CoFe_2O_4$ nanoparticles [3]. The corresponding SAED patterns shown in Fig. 3 (right) demonstrate the polycrystalline of $CoFe_2O_4$ nanoparticles with a spinel-type structure. The increase of calcination temperature results in more intense spots in the electron diffraction rings. The sample calcined at 900 °C shows a stronger spotty-ring electron diffraction pattern than those calcined at 700 and 800 °C. This result indicates that the larger particle size results in the higher crystallinity of $CoFe_2O_4$ nanoparticles [23]. From the diffraction rings, the type of crystal structure can be determined by measuring the ring radii (R). The distance between successive planes (d) in each sample is calculated using the equation $d = (\lambda L/R)$, where λ is the electron wavelength and L is the camera length [5]. The results of the calculated d spacing of the samples calcined at 700, 800 and 900 °C are in agreement with those reported in the standard data JCPDS no.78-1970.

Figure 4 shows the optical absorption spectra of $CoFe_2O_4$ nanoparticles calcined in the temperature range of 700–900 °C The samples were chosen because these samples have high crystallinity in comparison with $CoFe_2O_4$ calcined at 650 °C. In the figure, the strong absorption band spectra of the samples calcined at 700, 750, 800 and 900 °C

are centered at 269.87, 273.19, 273.52 and 276.06 nm, respectively. The increase of absorption band spectra with increasing calcination temperature is contributed to the decrease of electronic transition energy resulting from two types of charge transfer: (1) the 2p state of O to the 3d state of transition metals and (2) the 3d to 3d state of transition metals occupied in tetrahedral (A) and octahedral (B) intersublattice sites [24, 26]. Since inverse spinels have a direct band gap (E_g) [27], the value of E_g for the $CoFe_2O_4$ nanoparticles can be evaluated using the Tauc and Davis-Mott model by extrapolating the plots of $(\alpha h\nu)^2$ versus ($h\nu$) to the zero value of $(\alpha h\nu)^2$, where α is the absorption coefficient, h is the Plank constant, and ν is the frequency of the incident radiation [4, 28, 29]. The results of these plots are shown in Fig. 5 and the obtained values for the direct band gap of all samples calcined at different temperatures are listed in Table 1. The correlated band gaps of the samples calcined at 700, 750, 800 and 900 °C are 4.3, 3.4, 3.4, and 3.0 eV, respectively. It is obvious that the value of E_g tends to be decreased with increasing crystallite size. This approach result is in good agreement with those reported by many research groups in various metallic oxides such as CeO, ZnO, Ag_2O, and Si [23, 30, 32]. However, the obtained E_g values of the $CoFe_2O_4$ nanoparticles in our work are quite different from the bulk $CoFe_2O_4$ (2.7 eV) and others reported in literature. For instance, Holinsworth et al. [24] reported a direct band gap value of ∼2.7 eV in epitaxial $CoFe_2O_4$ films grown by pulsed laser deposition. Gaikwad et al. [33] reported a direct band gap of ∼2.6 eV in nanocrystalline $CoFe_2O_4$ films prepared by electrostatic spray pyrolysis (ESP) method. The blue shift of the absorption edge observed in the samples with different particle sizes can be explained on the basis of quantum confinement effect [23, 24] As the particle size becomes smaller and comparable to exciton Bohr radius of the material, the energy levels are discrete and electrons and holes are confined in a potential well, which is inversely proportional to the square of the radius of the particle [26]. As a result, a decrease in the nanocrystal size and an increase of the effective width of the E_g are observed.
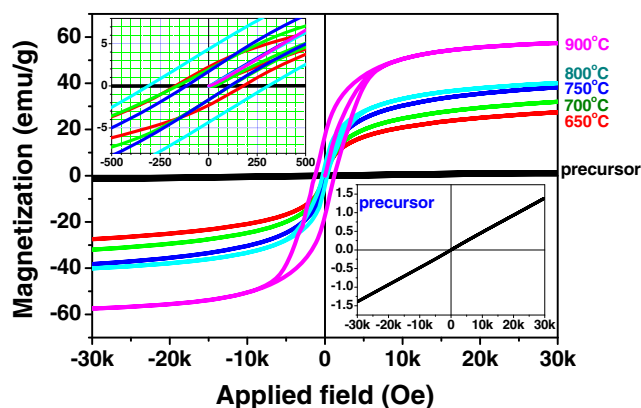

Fig. 6 Room temperature $M–H$ hysteresis loops of the $CoFe_2O_4$ precursor and nanoparticles calcined at 650, 700, 750, 800, and 900 °C
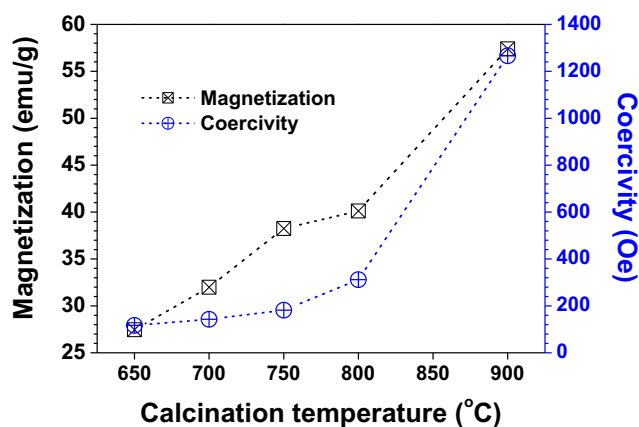
Fig. 7 Variation of specific magnetization (M) at the maximum H-field and coercivity (H_c) of the nanocrystalline $CoFe_2O_4$ powders as a function of calcination temperature

The results of room temperature magnetic properties, specific magnetization (M) and coercivity (H_c) of the $CoFe_2O_4$ precursor and nanoparticles under the applied field of ± 30 kOe are shown in Fig. 6. As can be seen in the inset in the lower right of the figure, the as-prepared precursor powder shows paramagnetism while the calcined samples exhibit ferrimagnetic behavior. The hysteresis curves exhibit a narrow hysteresis loop, corresponding to soft ferromagnetism of the samples calcined at temperatures below 800 °C in the field range of ± 0.5 kOe (see the upper left inset), while outside this range, the specific magnetization is increased with increasing magnetic field and it does not saturate within ± 30 kOe. At the maximum magnetic field, the specific magnetization (M_{max}) of the samples calcined at 650, 700, 750, 800, and 900 °C are 27.46, 31.99, 38.25, 40.11, and 57.40 emu/g, respectively. The coercivity values of 116.88, 142.86, 181.82, 311.69, and 1266.24 Oe are observed in the $CoFe_2O_4$ samples calcined at 650, 700, 750, 800, and 900 °C, respectively. The variation of M_{max} and H_c with calcination temperatures is shown in Fig. 7. It is clear that there is a tendency to enhance the magnetization with increasing of calcination temperature and particle size. This is attributed to the incomplete crystallization and small particle size after calcination at low temperature [22]. The effect of particle size on magnetic properties of ferrite materials can be described using the surface spin disorder in magnetic nanoparticles. The canted spin on the particle surfaces, having multiple configurations for any orientation of the core magnetization, is an important factor on the magnetic moment reduction [19, 35]. In addition, the surface is likely to behave as an inactive and dead layer with inconsiderable magnetization [19]. Consequently, M_{max} decreases for small-sized particles. In the present work, the M_{max} value varies between 27.46 and 57.40 emu/g obtained from the samples calcined at different temperatures in the range

of 650–900 °C and is particularly low in comparison with the room temperature saturation magnetization (80.8 emu/g) of the bulk $CoFe_2O_4$ [36]. The low value of M_{max} can be ascribed to the surface effect of nanoparticle and poor crystal structure of the prepared $CoFe_2O_4$ powders. However, the values of room temperature magnetization of our samples are higher than those reported for the $CoFe_2O_4$ nanoparticles [37].

As can be seen from the plot of coercivity depicted in Fig. 7, the H_c value gradually increases with increasing calcination temperature from 650 up to 800 °C, corresponding to the increase of particle size from 3.6 to 6.9 nm, and then the value rapidly increases to the maximum value of 1266.24 Oe in the sample with a crystallite size of 21.7 nm. The variation of H_c with particle size can be explained on the basis of the domain structure, critical diameter, and anisotropy of the crystal. Moreover, a crystallite will spontaneously break up into a number of domains in order to reduce the large magnetization energy that it would have if it were a single domain [38]. The increasing tendency of H_c with particle size may be because their sizes are within the range of a single domain size limit for $CoFe_2O_4$ (~ 60 nm), where the magnetization proceeds by reversible spin rotation at high applied magnetic field [39].

4 Conclusions

$CoFe_2O_4$ nanoparticles have been successfully synthesized by reverse micelle microemulsion method. The particles calcined in the temperature range of 650–900 °C are nanocrystalline with a spinel ferrite structure. The average crystallite size of the calcined samples was in the range of 3.6–21.7 nm. The estimated direct band gaps were 4.3, 3.4, 3.4 and 3.0 eV for the samples calcined at 700, 750, 800 and 900 °C, respectively. The increase of energy band gap with decreasing particle size indicates the existence of a quantum confinement effect in $CoFe_2O_4$ nanoparticles. All samples behave ferrimagnetism with the highest magnetization of 57.40 emu/g, and the highest coercivity of 1266.24 Oe was observed in a sample calcined at 900 °C. From the optical and magnetic properties of the obtained $CoFe_2O_4$ nanoparticles calcined above 750 °C, the materials may have the potential to be developed and used as a magnetically separable photocatalyst for wastewater treatment.

References

1. Sugimoto, M., Am, J.: Ceram. Soc. **82**, 269 (1999)
2. Safarik I., Safarikova M.: In: Hofmann, H., Rahman, Z., Schubert, U. (eds) Nanostructured materials, pp. 1e23. Springer Wien (2002)
3. Laokul, P., Amornkitbamrung, V., Seraphin, S., Maensiri, S.: Curr. Appl. Phys. **11**, 101 (2011)
4. Reetz, M.T., Maase, M.: Adv. Mater. **11**, 773 (1999)
5. Singhal, S., Sharma, R., Singh, C., Bansal, S.: Indian J. Mater. Sci. **2013**, 1–6 (2013)
6. Su, M. et al.: J. Hazard Mater. **95**, 211–212 (2012)
7. Rashad, M.M., Mohamed, R.M., Ibrahim, M.A., Ismail, L.F.M., Abdel-Aal, E.A.: Adv. Powder. Tech. **23**, 315 (2012)
8. Zhu, Z., Li, X., Zhao, Q., Shi, Y., Li, H., Chen, G.: J. Nanopart. Res. **13**, 2147 (2011)
9. Hunyek, A., Sirisathitkul, C., Harding, P.: Adv. Mater. **659**, 93–34 (2010)
10. George, M., John, A.M., Nair, S.S., Joy, P.A.: J. Magn. Mater. **302**, 190 (2006)
11. Yeong, K., Don, K., Choong, L.: Physical B **42**, 337 (2003)
12. Zhang, Y., Yang, Z., Yin, D., Liu, Y., Fei, C., Xiong, R., Shi, J., Yin, G.: J. Magn. Magn. Mater. **332**, 3475 (2010)
13. Juan, Y., Shaobo, M., Jiaorong, N., Wenxuan, C., Xinyu, S., Jiming, H., Guangming, H., Tonga, H.: Coll. Surf. A **340**, 109 (2009)
14. Elliott, D.W., Zhang, W.X.: Environ. Sci. Technol. **35**, 4922 (2001)
15. Subhasis, R., John, P., Baldev, R.: J. Mater. Chem. Phys. **124**, 264 (2010)
16. Husein, M.M., Nassar, N.N.: Curr. Nanosci. **4**, 370 (2008)
17. Zhao, L. et al.: J. Solid State Chem. **181**, 245 (2008)
18. Zori, M.H.: J. Inorg. Organomet. Polym. **21**, 81 (2011)
19. Naseri, M.G., Saion, E.B., Ahanger, H.A., Hashim, M., Shaari, A.H.: Powder Technol. **212**, 80 (2011)
20. Suryanarayana, C., Norton, M.G.: X-ray diffraction: a practical approach. Plenum Press, New York (1998)
21. Choodamadi, C., Nagabhushana, G.P., Rudraswamy, B., Chandrappa, G.T.: Mater. Lett. **116**, 227 (2014)
22. Chen, Y., Ruan, M., Jiang, Y.F., Cheng, S.G., Li. W.: J. Alloy. Compd. **493**, L36 (2010)
23. Maensiri, S. et al.: Cryst. Growth Des. **7**(5), 950 (2007)
24. Holinsworth, B.S. et al.: App. Phys. Lett. **103**, 82406 (2013)
25. Meinert, M., Reiss, G.: J. Phys. Condens. Matter **26**, 115503 (2014)
26. Zhang, Q.C., Yu, Z.H., Li, G., Ye, Q.M., Lin, J.H.: J. Alloy. Comp. **477**, 81 (2009)
27. Wei, S.H., Zhang, S.B.: Phys. Rev. B **63**, 045112 (2001)
28. El-Hagary, M., Matar, A., Shaaban, E.R., Emam-Ismail, M.: Mater. Res. Bull **48**, 2279 (2013)
29. Wang, X., Zhang, Y., Wu, Z.: Mater. Lett. **64**, 486 (2010)
30. Manzoor, U., Islam, M., Tabassam, L., Rahman, S.U.: Physica E **41**, 1669 (2009)
31. Banerjee, S., Maity, A.K., Chakravorty, D.: J. Appl. Phys. **87**(12), 8541 (2000)
32. Kim, T.W., Cho, C.H., Kim, B.H., Park, S.J.: Appl. Phys. Lett. **88**, 23102 (2006)
33. Gaikwad, R.S., Chae, S.Y., Mane, R.S., Han, S.H., Joo, O.S.: Int. J. Electrochem. **2011**, 1–6 (2011)
34. Ahmed, S.R., Kofinas, P.: Macromolecules **35**, 3338 (2003)
35. Kodama, R.H., Berkowitz, A.E., Mcniff, E.J., Foner, S.: Phys. Rev. Lett. **77**, 394 (1996)
36. Sharifi, I., Shokrollahi, H., Doroodmand, M.M., Safi. R.: J. Magn. Magn. Mater. **324**, 1854 (2012)
37. Rajendran, M. et al.: J. Magn. Magn. Mater. **232**, 71 (2001)
38. Cullity B.D.: Introduction to magnetic materials. Reading, Addison-Wesley Publishing Company, Reading, Massachusetts (1972)
39. Gajdhiye, N.G., Prasad, S., Balaji, G.: IEEE Trans. Mang. **35**, 2155 (1999)